I. INTRODUCTION

Cold nuclear matter effects are an essential ingredient in the perturbative quantum chromodynamics (QCD) description of hard processes in lepton-nucleus, proton-nucleus and nucleus-nucleus collisions. Of particular interest is their theoretical derivation form first principles. Specifically, in what follows we will discuss a picture where they arise from the collisional [1, 2], coherent [3] and inelastic [4] initial-state and final-state parton interactions in dense nuclear matter. Cold nuclear matter effects are reflected in hard probes observables even when final-state parton and hadron interactions in the quark-gluon plasma (QGP) dominate. dominate [5, 6]. In what follows we will concentrate in the simpler $e+A$ and $p+A$ reactions where QGP is not formed.

In d+Au collisions at the Relativistic Heavy Ion Collider (RHIC) a large suppression of particle production at large forward rapidity is observed [7]. STAR experimental data on π^0 attenuation at $y = 4$, for example, can be fitted with disparate models that emphasize either large shadowing or large nuclear stopping. A more realistic calculation [8] that includes the Cronin effect, high-twist shadowing, and initial-state energy loss - all independently constrained in different processes and center of mass energies - is presented in Figure 1. Our results show that both coherent and inelastic scattering on the nucleus have comparable impact on the observed cross section attenuation in this kinematic range. This finding stresses once again the need to identify and reliably evaluate experimental observables that are clean and sensitive signatures of jet interactions in cold nuclear matter.

Since d+A reactions involve both initial-state and final-state interactions of the parton (before and after the large Q^2 scattering), carefully selected processes (such as the Drell-Yan process) and semi-inclusive deeply inelastic scattering (SDIS) are needed to disentangle the physics. One example, muon pair production from the Fermilab E772/E886 experiment [9], is presented in Figure 2. Drell-Yan data and theoretical simulations are presented as the ratio of the differential cross sections on two different targets in minimum bias p+A reactions scaled down to a binary nucleon-nucleon interaction:

$$\text{Ratio}(A/B) \equiv R_{AB}^{DY} = B \cdot \frac{d\sigma_{pA}^{DY}}{dx_F dQ^2} \Big/ A \cdot \frac{d\sigma_{pB}^{DY}}{dx_F dQ^2} \ . \quad (1)$$

We considered two different invariant mass ranges 4 GeV $< Q <$ 5 GeV (left panels) and 6 GeV $< Q <$ 7 GeV (right panels). We also included two different ratios: R_{WD}^{DY} and R_{WBe}^{DY} in the top and bottom panels, respectively. The dashed lines represent a calculation of the cross section ratios that incorporates a leading twist-shadowing parametrization. The solid lines show our simulation with initial-state energy loss [4] that is compatible with the theoretical description of RHIC d+A and A+A data [5, 6]. Careful selection of the beam energy in fixed target experiments will allow for the easy separation of shadowing versus initial-state energy loss effects for the Drell-Yan process [8].

II. MEDIUM-INDUCED PHOTON BREMSSTRAHLUNG

Conversely, final-state interactions should ideally be studied at a dedicated electron-ion collider. For the remainder of this contribution, we will focus on the final-state medium induced photon bremsstrahlung [10] and

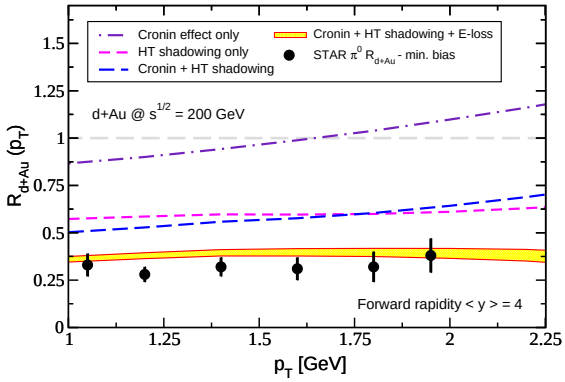

FIG. 1. Neutral pion suppression in minimum bias d+Au collisions at $y = 4$ at RHIC. Theoretical calculations that include known nuclear matter effects are shown. A complete simulation gives a good description of the experimental data.

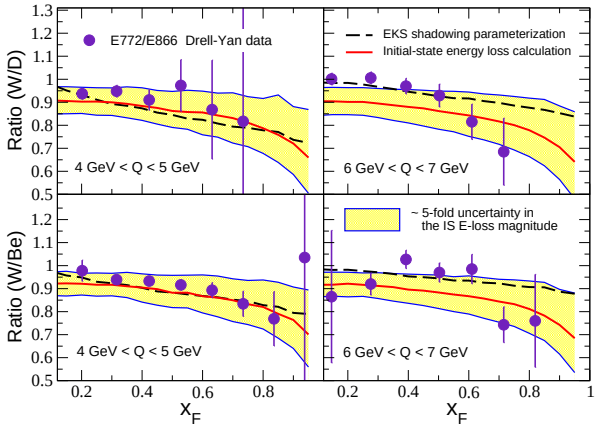

FIG. 2. Plot of the ratio of the dimuon cross section σ(p+W)/σ(p+A), where A = D,Be, from both experiment and theory for 800 GeV protons colliding with a fixed nuclear target. The theory curves are the NLO Drell-Yan cross section calculation, including shadowing effects and initial-state energy loss, respectively. The yellow bands indicate a five-fold variation of the mean quark medium-induced energy loss.

the similarities and differences between cold nuclear matter and the QGP.

The computation of photon bremsstrahlung is usually considered to be easier than that of gluon bremsstrahlung due to the absence of self-interactions of the gauge boson. However, it is not well appreciated that the two physics processes are quite different. We consider the scattering of a fast quark in nuclear matter is modeled via interactions with an external non-Abelian field $V^{\mu,c}(q)$:

$$V^{\mu,c}(q) = n^\mu\, 2\pi\delta(q^+)\, V^c(q)\, e^{iq\cdot z}\ ,$$
$$g_s V^c(q) \equiv v(q)\, T^c(t)\ . \qquad (2)$$

Here, the four-vector $n^\mu = \delta^{\mu,-} = [0, 1, \mathbf{0}_\perp]$ and the color matrix $T^c(t) \in \mathrm{SU_c}(3)$ in Eq.(2) represents the target charge that creates the non-Abelian field. We take the Fourier transform $v(q)$ to be of color-screened Yukawa type but with Lorentz boost invariance:

$$v(q) \equiv \frac{4\pi\alpha_s}{-q^{\,2}+\mu^2} = \frac{4\pi\alpha_s}{\mathbf{q}_\perp^{\,2}+\mu^2} = v(\mathbf{q}_\perp)\ , \qquad (3)$$

where we have used the $q^+ = 0$ choice of frame. This specific form of $v(q) = v(\mathbf{q}_\perp)$ is particularly useful since in-medium interactions in both hot and cold nuclear matter are of finite range $r_{int.} = \mu^{-1}$ and we shall assume that $\lambda\mu \gg 1$, where λ is the quark mean free path.

The radiative matrix element, which arises form the quark scattering at position z_i, is illustrated in Fig. 3 reads:

$$\mathcal{M}_{rad}(k,\{i\}) = e\left(\frac{\epsilon\cdot p_f}{k\cdot p_f} - \frac{\epsilon\cdot p_i}{k\cdot p_i}\right) e^{iz_i^+ k^-}\ . \qquad (4)$$

In Eq. (4) the collisional amplitude is not shown. Let the initial- and final-state momenta of a fast on-shell quark be $p_i = [E^+, Q^2_{\perp\, i-1}/(2E^+), \mathbf{Q}_{\perp\, i-1}]$, $p_f = [E^+, Q^2_{\perp\, i}/(2E^+), \mathbf{Q}_{\perp\, i}]$, such that $\mathbf{Q}_{\perp\, i} - \mathbf{Q}_{\perp\, i-1} = \mathbf{q}_{\perp\, i}$. Note that for asymptotic initial-state and final-state quarks the double Born term dies not contribute since

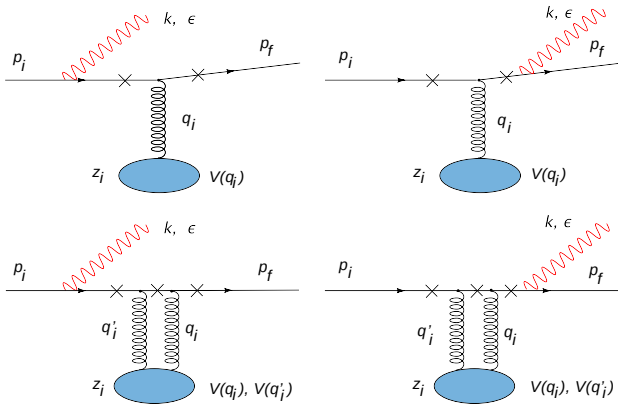

FIG. 3. Top panel: single-Born diagrams for medium-induced γ emission. Bottom panel: the corresponding double-Born diagrams in the $z_{i'} \to z_i$ limit. We denote by " $\times$" the propagators that enter the calculation.

$\mathbf{q}_\perp + \mathbf{q}'_\perp = 0$, and $p_i = p_f$ The double differential medium-induced photon distribution is then given by:

$$k^+\frac{dN^\gamma(k;\{i\})}{dk^+ d^2\mathbf{k}_\perp} = \frac{1}{2(2\pi)^3}|\mathcal{M}_{rad}(k,\{i\})|^2$$
$$= \frac{\alpha_{em}}{\pi^2}\frac{\left(\frac{k^+}{E^+}\right)^2 \mathbf{q}^2_{\perp\, i}}{\left(\mathbf{k}_\perp - \frac{k^+}{E^+}\mathbf{Q}_{\perp\, i-1}\right)^2\left(\mathbf{k}_\perp - \frac{k^+}{E^+}\mathbf{Q}_{\perp\, i}\right)^2}\ , \qquad (5)$$

and is dominated by emission coincident with the directions of the incoming and the outgoing quarks. Changing variables $\kappa = \mathbf{k}_\perp - \mathbf{k}_\perp^{(\mathrm{pole})}$, $\mathbf{k}_\perp^{(\mathrm{pole})} = \mathbf{Q}_{\perp\, i}k^+/E^+, \mathbf{Q}_{\perp\, i-1}k^+/E^+$, respectively, we obtain the QED double logarithmic result:

$$N^\gamma(\{i\}) \approx 2\frac{\alpha_{em}}{\pi}\ln\frac{k^+_{\max}}{k^+_{\min}}\ln\frac{q^2_{\max}}{m^2}\ , \qquad (6)$$

where m^2 regulates the collinear divergence.

The evaluation of the final-state medium-induced photon bremsstrahlung is more involved. Here, the destructive interference between the photons induced by the hard scattering and the subsequent interactions in QCD matter must be accounted for. Taking into account the interactions of the parent quark along its trajectory through the QGP and the average over the transverse momentum transfers, the main theoretical result reads [10]:

$$k^+\frac{dN^\gamma(k)}{dk^+ d^2\mathbf{k}_\perp} = \frac{\alpha_{em}}{\pi^2}\Bigg\{\int\frac{d\Delta z_1}{\lambda_q(z_1)}\int d^2\mathbf{q}_{\perp\,1}\frac{1}{\sigma^{\mathrm{el}}}\frac{d^2\sigma^{\mathrm{el}}}{d^2\mathbf{q}_{\perp\,1}}$$
$$\times\left[|\mathcal{M}_{rad}(\{1\})|^2 + 2\mathcal{M}^*_{rad}(\{1\})\mathcal{M}_{rad}(\{0\})\cos(k^-\Delta z_1^+)\right]$$
$$+\prod_{i=1}^{2}\left[\int\frac{d\Delta z_i}{\lambda_q(z_i)}\int d^2\mathbf{q}_{\perp\, i}\frac{1}{\sigma^{\mathrm{el}}}\frac{d^2\sigma^{\mathrm{el}}}{d^2\mathbf{q}_{\perp\, i}}\right]$$
$$\times 2\mathcal{M}^*_{rad}(\{2\})\mathcal{M}^*_{rad}(\{1\})\cos(k^-\Delta z_2^+)\Bigg\}\ . \qquad (7)$$

In Eq. (7) $\Delta z_i^+ = z_i^+ - z_{i-1}^+$, the Δz_i integrals are nested, and $\tau_f^{-1} \approx 2k^- = \mathbf{k}^2/k^+$ is the inverse photon formation time. When $\tau_f^{-1}\lambda \gg 1$ the photons decohere early from the parent quark and our result reduces to incoherent emission from individual scattering centers. Our result treats the case of finite $L/\lambda_q \sim$ few, relevant to heavy ion physics. Second, we find that the most significant contribution to the Landau-Pomeranchunk-Migdal (LPM) effect [11, 12] for photons comes from the interference of the medium-induced photon radiation with the hard emission from the large Q^2 scattering of the parent quark. Finally, we find that there can be non-linear corrections $\sim L^2$ to the dominant linear in L behavior of the photon spectrum.

We are now ready to study numerically the final-state medium-induced photon spectrum. Our results are limited to first order in opacity. With Eq. (4) representing the amplitude of both light and heavy fermions, the intensity spectrum is easily generalized to quarks

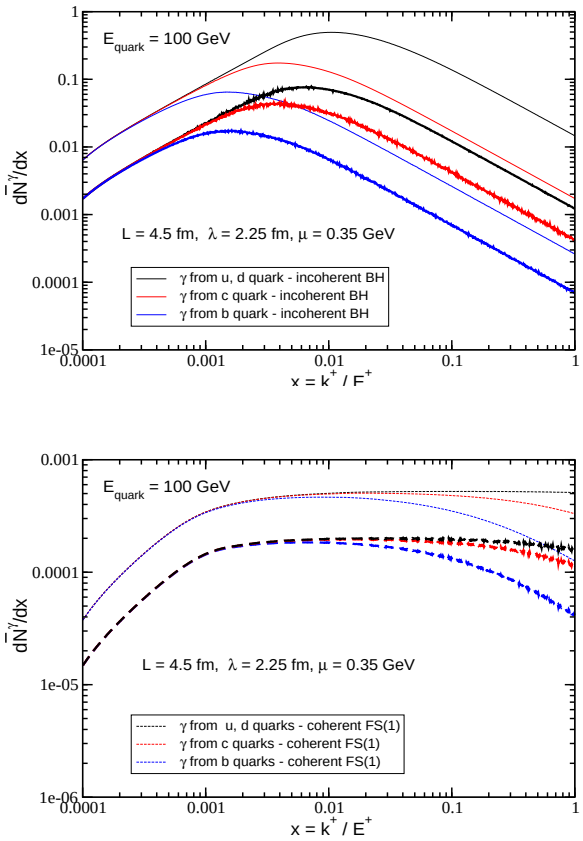

FIG. 4. Top panel: medium-induced photon number spectrum versus $x = k^+/E^+$ for $E_q = 100$ GeV light, charm and bottom quarks. Thin lines refer to central Au+Au collisions at $\sqrt{s} = 200$ GeV. Thick lines correspond to cold nuclear matter of length $L = 4.5$ fm. We show the incoherent Bethe-Heitler spectrum. Bottom panel: same as above, but for the coherent photon production induced by the in-medium interactions of a quark jet produced in a large Q^2 scattering process.

with physical and dynamical in-medium mass, $m^2 = M_q^2 + m_{\rm eff.}^2$. For the case of cold nuclear matter we select $L = 4.5$ fm, $\mu = 0.35$ GeV and $\lambda_q = 2.25$ fm. Also, $m_{\rm eff.} = m_N$. For the QGP case we show an example of a quark propagating outwards from the center of the medium created in $b = 3$ fm Au+Au collisions at RHIC. The top panel of Fig. 4 shows the medium-induced photon number spectrum $d\bar{N}^\gamma/dx = (e/e_q)^2 dN^\gamma/dx$, $x = k^+/E^+$, normalized by the squared fractional quark electric charge (bar will denote such scaling for any physics quantity). We considered light, $M_{u,d} = 0$ GeV, and heavy, $M_c = 1.5$ GeV, $M_b = 4.5$ GeV, quarks of energy $E_q = 100$ GeV in the Bethe-Heitler limit. Thick lines represent our calculation in cold nuclear matter. This lines give the QGP result for reference. Note that for the same L/λ_g the difference is only a factor of several. The shape of the photon spectra are similar but the emitted photons are softer on average in cold nuclear matter.

The bottom panel of of Fig. 4 shows the final-state spectrum with the LPM destructive interference effect included in the calculation. In contrast to the case of non-abelian bremsstrahlung [4], for photons the soft part of the spectrum is more strongly suppressed. A difference in the magnitude of the spectrum, similar to the case of Bethe-Heitler radiation, remains between the cold nuclear matter and the QGP case.

To determine whether effective field theory techniques [13] can improve precission of the calculatioins of paton propagation in cold nuclear matter and to develop a consistent picture of jet and particle production in SDIS will be a high priority for us in preparation for the physics program at the future EIC.

[1] A. Accardi, arXiv:hep-ph/0212148.
[2] I. Vitev, Phys. Lett. B **562**, 36 (2003).
[3] J. W. Qiu and I. Vitev, Phys. Lett. B **632**, 507 (2006).
[4] I. Vitev, Phys. Rev. C **75**, 064906 (2007).
[5] R. Sharma, I. Vitev and B. W. Zhang, Phys. Rev. C **80**, 054902 (2009) [arXiv:0904.0032 [hep-ph]].
[6] I. Vitev and B. W. Zhang, Phys. Rev. Lett. **104**, 132001 (2010) [arXiv:0910.1090 [hep-ph]].
[7] J. Adams *et al.* [STAR Collaboration], Phys. Rev. Lett. **97**, 152302 (2006) [arXiv:nucl-ex/0602011].
[8] R. B. Neufeld, I. Vitev and B. W. Zhang, arXiv:1010.3708 [hep-ph].
[9] M. B. Johnson *et al.* [FNAL E772 Collaboration], Phys. Rev. Lett. **86**, 4483 (2001) [arXiv:hep-ex/0010051].
[10] I. Vitev and B. W. Zhang, Phys. Lett. B **669**, 337 (2008) [arXiv:0804.3805 [hep-ph]].
[11] L. D. Landau and I. Pomeranchuk, Dokl. Akad. Nauk Ser. Fiz. **92**, 535 (1953).
[12] A. B. Migdal, Phys. Rev. **103**, 1811 (1956).
[13] G. Ovanesyan, I. Vitev, in preparation.